Comprehensive Modeling of Electromigration Induced Interconnect Degradation Mechanisms

H. Ceric, R. Lacerda de Orio, and S. Selberherr

Abstract— **The reliability requirements on modern interconnect and the physical complexity of electromigration phenomena demand close and systematic application of experimental and TCAD based methods for the assessment of interconnect failure and the development of sophisticated layout design rules. We present and discuss state-of-the art electromigration models for both phases of failure development: void nucleation and void evolution. The discussion includes the role of copper microstructure, mechanical stress, capping layer, and void nucleation conditions. A concept for usage of the presented models for prediction of time-to-failure in three-dimensional interconnect geometries is given and demonstrated on examples. The results of simulations are discussed and verified with results of accelerated interconnect testing.**

I. Introduction

Continuous shrinking of the dimensions of on-chip interconnects and the introduction of advanced backend-of-line (BEoL) manufacturing process steps increases the complexity of physical phenomena behind the common electromigration failure scenario. The total wiring length amounts to kilometers arranged in up to ten levels with hundreds of milions of interlevel connections. The tendency of modern technologies toward increasing interconnect length and at the same time reducing its cross section makes interconnect layout more and more susceptible to electromigration.

Since electromigration first gained importance for microelectronics backend technology, the army of engineers, physicists, and material scientists have tried to understand and model the underlaying phenomena. The necessity to reduce the electromigration risk was huge from the very beginning and with the introduction of new technologies it is even more increasing. Because the phenomenon does not manifest itself until a circuit has been operated for months, or even years, electromigration cannot be prevented by product testing. An ultimative hope of integrated circuits designers today is to have a computer program at hand which predicts the behavior of thin film metallizations under any imaginable condition. Contemporary integrated circuits are often designed using simple and conservative design rules to ensure that the resulting circuits meet reliability goals. This precaution leads to reduced performance for a given circuit and metallization technology.

The main challenge in electromigration modeling and simulation is the diversity of the relevant physical phenomena. Electromigration induced material transport is also accompanied by material transport driven by the gradients of material concentration, mechanical stress, and temperature distribution. A comprehensive, physics based analysis of electromigration for modern copper interconnect lines serves as the basis for deriving sophisticated design rules which will ensure higher steadfastness of interconnects against electromigration.

Relaying of previous work we present a model which reveals an improvement in two mayor points. First there is a complete integration of mechanical stress phenomena in the connection with microstructural aspects in the classical multi-driving force continuum model and, secondly, a newly developed finite element based scheme enables an efficient numerical solution of the three-dimensional formulation of the problem while the physical soundness is preserved. A satisfying assessment of electromigration reliability can only be achieved through a combination of experimental methods and the utilization of TCAD tools. Therefore, we also discuss a possible usage scenario of TCAD tools in connection with results of accelerated interconnect tests.

II. Physics Based Modeling

Generally, the evolution of electromigration induced failure consists of two phases. In the first phase which we call the void nucleation phase, the interconnect materials undergo an inner transformation followed by build-up of mechanical stress, which leads to the formation of an initial void. In this phase no significant change in the interconnect resistance can be observed. This phase is followed by the void evolution phase in which the void can be observed on SEM and TEM pictures. A resistance change in this phase can still be hardly observed. The situation changes when a void moves to a position inside the interconnect, where the geometrical constellation causes that even a small void and its evolution induces a large resistance change. Another scenario of the rapid resistance change is when the local geometrical conditions enhance a rapid void growth.

If we denote the void nucleation time with t_N and the void evolution time with t_E, the time-to-failure (TTF)

H. Ceric, R. Lacerda de Orio, and S. Selberherr are with the Institute for Microelectronics, Technical University Vienna, Gußhausstraße 27-29, 1040 Wien, Austria, E-mail: {Ceric|Orio|Selberherr}@iue.tuwien.ac.at

978-1-4244-1881-7/08/$25.00 © 2008 IEEE

t_F is,

$$t_F = t_N + t_E. \quad (1)$$

The theoretical models of electromigration and accompanied driving forces of material transport have gone through a long evolution starting with early works of Blech *et al.* [1], [2], [3], over very substantial contributions of Mullins [4], Korhonen *et al.* [5], Lloyd *et al.* [6], [7], and Clement [8], to general contemporary models of Sarychev *et al.* [9] and Sukharev [10], [11], [12].

A. Bulk Vacancy Transport

The bulk vacancy transport is given by the following balance equation

$$\mathbf{J}_v = -\mathbf{D}\Big(\nabla C_v + \frac{Z^* e}{k_B T} C_v \nabla\varphi + \frac{f\Omega}{3\, k_B T} C_v \nabla \mathrm{tr}(\bar{\bar{\sigma}})\Big), \quad (2)$$

$$\frac{\partial C_v}{\partial t} = -\mathrm{div}\mathbf{J_v}. \quad (3)$$

Residual process stresses, thermo-mechanical stresses, and electromigration induced stresses cause anisotropy of material transport and therefore a tensorial diffusivity $\mathbf{D}$ must be taken into account. Along the fast diffusivity paths, such as grain boundaries and interfaces to capping and barriers layer, higher diffusivities have to be assumed. The divergence of the vacancy flux produces local strain

$$\frac{\partial \varepsilon^v_{ij}}{\partial t} = \Omega(1-f)\mathrm{div}\mathbf{J_v}\delta_{\mathbf{ij}}, \quad (4)$$

which is equlibriated by induced displacements $\mathbf{u} = \mathbf{u}(u_1, u_2, u_3)$ in the copper bulk according to the Lame equations,

$$\mu\Delta u_i + (\mu+\lambda)\frac{\partial}{\partial x_i}(\nabla\mathbf{u}) = B\frac{\partial \mathrm{tr}(\bar{\bar{\varepsilon}}^{\mathrm{v}})}{\partial x_i}, \quad i = 1,2,3 \quad (5)$$

Here, elastic deformation of the metal is assumed

$$\sigma_{ij} = \sum_{ijkl} \mathbf{C}_{kl}\varepsilon_{kl}, \quad (6)$$

with small displacement approximations,

$$\varepsilon_{ij} = \frac{1}{2}\Big(\frac{\partial u_i}{\partial x_j} + \frac{\partial u_j}{\partial x_i}\Big), \quad i,j = 1,2,3. \quad (7)$$

The simplest way to include an effect of the grain boundaries as a site of vacancy production and annihilation is to use a Rosenberg-Ohring [13] term,

$$G = \frac{C_v - C_v^{eq}}{\tau}. \quad (8)$$

which is postulated on a basis of experimental observations. τ is declared to be the: "*life time of a vacancy in the presence of sinks*". A more physical interpretation of τ declares it as a characteristic relaxation time needed for the vacancy concentration to reach the level which is in local equilibrium with stress [10]. However, the full description of the atomic mechanism of vacancy generation and annihilation in grain boundaries goes beyond the capability of continuum modeling and can only be obtained by molecular dynamics methods [14].

B. Impact of Mechanical Strain on Electromigration

The choice of passivating film material and the corresponding process technology cause tensile or compressive stress in the interface between the passivating film and the interconnect metal. Interfacial compressive stress diminishes electromigration along interfaces by reducing diffusivity [15]. However, numerous experimental observations have shown [7], [6] that tensile stress in the interface increases the possibility of failure. Increased thickness and rigidity of the capping layer prevents relaxation of both thermal and electromigration induced stress, which results in dielectric cracking and metal extrusion.

The local stress state introduces an anisotropy of diffusivity. The dependence of the tensorial diffusivity on the stress state is given by following relationship:

$$D_{ij} = \frac{1}{2}\sum_{k=1}^{12} \mathbf{r}_i^k \mathbf{r}_j^k \Gamma^k, \quad (9)$$

where $\mathbf{r_i^k}$ is the jump vector for an arbitrary lattice site and Γ^k is the jump rate. Local stress modifies through strain ε the local jump rate in an anisotropic manner

$$\Gamma^k = \Gamma^0 \exp(-\varepsilon_I \Omega\,(\mathbf{C}\varepsilon)). \quad (10)$$

$\mathbf{C}$ is the elasticity tensor and $\varepsilon_{\mathbf{I}}$ is the strain induced by a single vacancy. The basis for this model, the relationship (9), was first presented in the theory of Dederichs *et al.* [16]. In conjuction with (10) we use (9) to model the capping-stress impact on the cumulative material transport given by (2).

For both, capping and barrier layer, the quality of adhesion between copper is of crucial importance. This adhesion quality can be influenced by choice of processes and materials, for example, the following combinations have been extensively investigated: Cu/TiW, Cu/SiO_2, TiW/Cu/TiW, W/Cu/TiW, SiO_2/Cu/TiW [17], [18]. Weak bonding between copper and the capping layer not only enhances electromigration prior to void nucleation but also speeds-up void evolution and growth. Observations showed that an epitaxy-like (e.g. uninterupted array of parallel lattice planes) transition between copper and capping strenghtens the copper/capping bonding [19].

III. Void Nucleation Condition

The basis for the current understanding of void nucleation is the work of Flinn [20], which considers a circular patch on the interface between copper and the capping layer with virtually no adhesion. Such an entity can actually be caused by a surface defect or contamination [21]. As the stress in the line increases, the free metal surface is driven to adopt an equilibrium, half-spherical shape, and a void embryo forms. The stress threshold given by Clemens *et al* [22]. and Glaixner *et al* [23] is:

$$\sigma_{th} = \frac{2\gamma_m \sin\theta_c}{R_p}. \qquad (11)$$

R_p is the radius of the adhesion-free patch and θ_c is the critical angle. For stresses $\sigma < \sigma_{th}$ an energy barrier exists between the embryo and a stable-growing void. If the stress is above the threshold value ($\sigma > \sigma_{th}$), the free energy monotonically decreases with void volume and the energy barrier vanishes. If we now assume the adhesion free patch with a radius of 10 nm (about 20 atoms) and $\theta_c = \pi/2$, we obtain $\sigma_{th} \approx 344$ MPa. In modern interconnects this stress level can already be reached by thermal stress [24].

The void nucleation time t_N is obtained (Section II-A) as the time needed for reaching the stress threshold given by (11).

IV. Modeling of Void Evolution Phase

When the stress level defined by (11) is reached at some interfacial spots where a flaw can be assumed, the failure development enters the next phase and a different modeling Ansatz must be applied. Here, we have an evolving void surface shaped by two dynamic forces: the chemical potential gradient and the electron wind. Including both contributions, electromigration and chemical potential-driven surface diffusion, gives the total surface vacancy flux $\mathbf{J_s} = J_s\mathbf{t}$, where $\mathbf{t}$ is the unit vector tangent to the void surface [25], [26], [27], [28]

$$J_s = -D_s\Big(eZ^*E_s + \Omega\nabla_s\Big(\frac{\bar{\bar{\sigma}} : \bar{\bar{\varepsilon}}}{2} - \gamma_s\kappa\Big)\Big). \qquad (12)$$

$E_s \equiv \mathbf{E_s}\cdot\mathbf{t}$ is the local component of the electric field tangential to the void surface, ∇_s is the surface gradient operator, $1/2\,(\bar{\bar{\sigma}} : \bar{\bar{\varepsilon}})$ is the strain energy density of the material adjacent to the void surface, and κ is the curvature of the void surface. D_s is given by an Arrhenius law:

$$D_s = \frac{D_0\,\delta_s}{k_B\,T}\exp\Big(-\frac{Q_s}{k_B\,T}\Big). \qquad (13)$$

δ_s is the thickness of the diffusion layer, Q_s is the activation energy for the surface diffusion, and D_0 is the pre-exponential coefficient for mass diffusion.

Numerical tracking of the surface is necessary, since it fully determines the failure dynamics. The shape of the voids together with local geometry conditions cause changes in the interconnect resistance and the speed of the void growth. The migration direction is strongly influenced by the shape of a void.

The three-dimensional algorithms for simulation of the void surface evolution are computationally very demanding, and currently no satisfactory solution exists. A simplified version of the two-dimensional successfuly applied diffuse interface model [27], [26] maybe a promising candidate for a solution.

V. Estimation of the Void Growth Time

Instead of using cumbersome tracking of void surfaces for the situations, where a void does not change its position after starting an intensive growth phase, a simplified diffusion interface method for the estimation of the void evolution time t_E can be applied. In the following we describe an example of such a method.

An initial void with some small radius r_0 is placed on some characteristic position inside the interconnect (Fig. 1). Since most of the fatal voids are nucleated in the vicinity or in the area of interconnect vias, we consider in particular these cases. The configurable initial void volume is V_0, which is smaller than $4\pi r_0^3/3$, because the void area is confined by its spherical surface and the boundary of the interconnect (Fig. 1). Starting from the initial void radius r_0, the void radius is gradually incremented r_0, $r_1 = r_0 + \Delta r_1$, $r_2 = r_1 + \Delta r_2, ...,$ with $\Delta r_1 \geq \Delta r_2 \geq ... \geq \Delta r_n$. For each void radius the electrical field in the interconnect structure is calculated by means of the finite element method using a diffuse interface approach. To obtain the distribution of the electrical potential inside the interconnects the Poisson equation has to be solved

$$\nabla\cdot(\gamma(\phi)\nabla\varphi) = 0\,. \qquad (14)$$

To impose correct boundary behavior of the electrical field on the spherical void surface a diffuse interface approach has been applied [26]. In this approach the electrical field in the metal and the void is calculated on the same finite element mesh. The electrical conductivity depends on the scalar field $\phi(x, y, z)$

$$\gamma(\phi) = \frac{\gamma_E[1 + \phi(x, y, z, t)]}{2}. \qquad (15)$$

In order to obtain sufficient accuracy the scalar field $\phi(x, y, z, t)$ must be resolved on a locally refined mesh (Fig. 2). For an electrical field calculated in such a way, the resistance of the interconnect via is also calculated [29], [30]. With growing void size the resistance increases. The whole process is stopped, when a void radius is reached for which $100\times(R_{actual}/R_{initial}-1) > 20\%$.

The primary driving force of material transport at the void surface is electromigration proportional to the tangent component of the current density (Fig. 3). Since the diffuse interface approach for the calculation of the current density ensures the correct physical behavior of the electrical field in the vicinity of the isolating void, the normal component of the current density on the void surface is always zero and we can use the formula

$$J_{m,i} = 2\frac{\int_V \|\mathbf{J}\|[1-\phi_i^2(x,y,z)]\,dV}{\int_V[1-\phi_i^2(x,y,z)]\,dV}, \qquad (16)$$

for the average current density over a void with radius r_i. (16) expresses the averaging of the current density weighted with the finite element volume inside the interconnect. Since $\phi_i(x,y,z) = 1$ in metal and $\phi_i(x,y,z) = -1$ in the void area, the term $1-\phi_i^2(x,y,z)$ is non-zero only in the void-metal interface area.

The evolution of the void is caused by material transport on the void surface and in the vincinity of the void surface. The mass conservation law gives the expression for the mean propagation velocity v_i of the evolving void-metal interface

$$v_i = \frac{D_v}{k_B\,T\,\gamma_E}\,eZ^*J_{m,i}, \qquad (17)$$

which is valid for all void shapes.

As we can see from Fig. 4, the average current density on the void surface increases with the void size. Both, current density and resistance, exibit a very similiar dynamic behavior. The transient resistance increase is in accordance with the measurement results presented in [31]. Compared with the earlier result [32], using the assumption of cubical void shapes, our approach enables more realistic simulations.

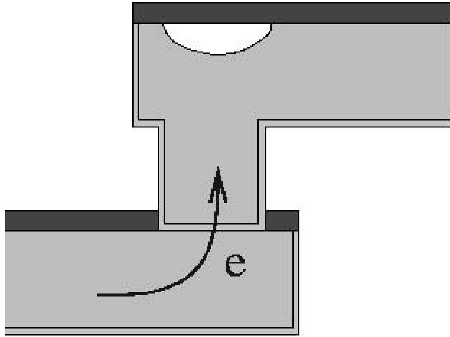

Fig. 1. Position of the growing void. Initial position and volume are chosen on the basis of experimental results.

An open question is how to use the obtained average current density (Fig. 4) for the estimation of the void growing time (t_E) up to the critical void size. In [32] a simple formula is suggested

$$t_E = \frac{V_c - V_0}{v_m A_s}. \qquad (18)$$

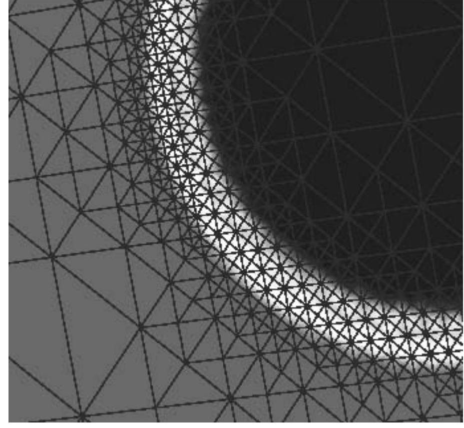

Fig. 2. Detail of the used locally refined mesh. $\phi = 1$ in the grey area and $\phi = -1$ in the black area.

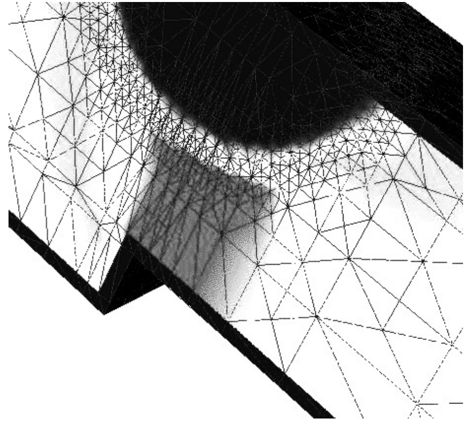

Fig. 3. Typical current density distribution picture in the vincinity of the spherical void. The grey area marks peak values of the current density.

In this equation V_c is the critical void size, V_0 is the initial void size, A_s is the cross section of the interconnect in the vincinity of the growing void, and v_m is the mean velocity of the evolving void-metal interface. However, this formula is only valid in the case of a cubical void which is a very rough approximation of the real situation.

According to the newer experimental results [33] the real void shape is significantly better approximated by a spherical sector. In this case t_E can be estimated as

$$t_E = \sum_i \frac{\Delta r_{i+1}}{v_i}, \qquad (19)$$

assuming that for sufficently small Δr_{i+1}, the void radius grows from r_i to r_{i+1} with a constant velocity v_i. As we can see from (17), the velocity v_i depends on the vacancy diffusivity D_v which itself has significantly varying values depending on the diffusion path.

The electromigration assisted self-diffusion of copper is a complex process which includes simultaneous

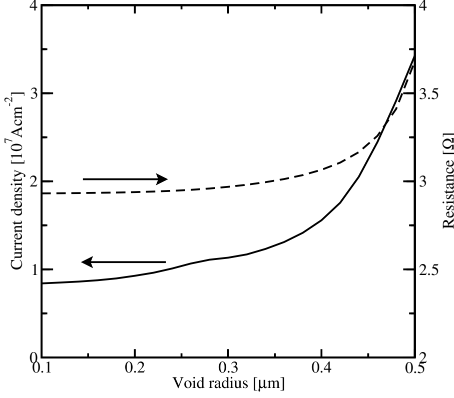

Fig. 4. Change of average current density and via resistance depending on the void radius.

diffusion through the crystal bulk, along grain boundaries, along the copper/barrier interfaces, and along the copper/cap-layer interface. Therefore, the diffusivity used in (17) must be a cumulative value as discussed in [34]

$$D_v = D_b + D_{gb}\Big(\frac{\delta_{gb}}{d}\Big) + D_{Cu/b}q_{Cu/b} + D_{Cu/N}q_{Cu/N}. \tag{20}$$

D_b, D_{gb}, $D_{Cu/b}$, and $D_{Cu/N}$ represent the diffusivity through the bulk, along the grain boundaries, copper/barrier interfaces, and copper/caplayer interfaces, respectively. δ_{gb} is the width of the grain boundary and d the average length of a grain boundary. The coefficients $q_{Cu/b}$ and $q_{Cu/N}$ depend only on the layout geometry. Within the limits set by experimentally determined values, the model calibration process described in the following section determines all relevant diffusivities appropriately.

VI. Usage Scenario for TCAD Tools

Simulation can be used as a tool for extrapolation of long time interconnect behavior on the basis of results of accelerated electromigration tests. This capability goes clearly beyond an extrapolation by standard statistical methods which rely on Black's equation and are able to predict TTF only for the particular interconnect geometry used in corresponding accelerated tests. The usage of TCAD tools enables a prediction of the behavior for structures which are obtained by variation of geometrical properties and operating conditions of a previously used initial test structure.

The assumed scenario for application of an electromigration reliability TCAD tool is:

- Model Calibration. For this purpose we use one layout and many test units. At the end of calibration all parameters of the model are fixed. During this process, different microstructures are considered and simulation parameters are varied with the goal to reproduce experimental failure time statistics, Fig. 5.
- Model Application. The calibrated model is used for simulation. The simulation extrapolates the behavior of the interconnect under real life conditions.

For the given interconnect layout and monocrystalline material, simulation will provide a unique time-to-failure. All impact factors, e.g. geometry of the layout, bulk diffusivity, interface diffusivity, and mechanical properties are deterministic and so the TTF is deterministic. However, the situation changes, when the inteconnect possesses a microstructure. The microstructure has a significant impact on electromigration, since it introduces a diversity of possible electromigration paths and local mechanical properties (the Young modulus and Poisson factor depend on the crystal orientation in each grain). However, the microstructure itself can not be completely controlled by process technology. In other words, the position of grain boundaries, angles in which they meet the interfaces, etc. can not be designed, the process itself determines only statistics of grain sizes and textures.

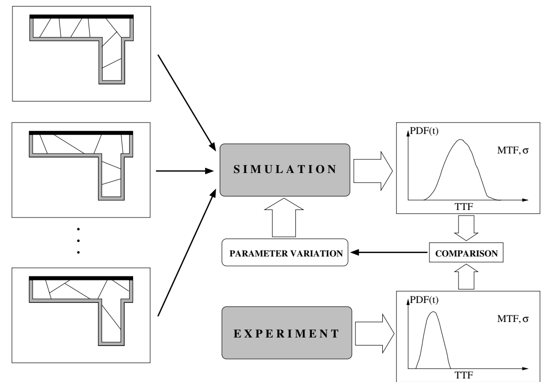

Fig. 5. Electromigration model calibration using a multitude of microstructural inputs.

If we extract statistical properties of the microstructure obtained by a specific process of a test structure and use these properties to design an input for simulation tools, the resulting time-to-failure distribution from the simulation with these inputs has to fit the experimental distribution. If this is not the case, the configurable parameters of the model have to be varied, until the experimental TTF distribution fits the simulated one. When a resonable agreement between experimentally determined TTF distribution and the simulated TTF distribution is reached, the TCAD tool is considered as calibrated and can be used for electromigration reliability assessment under realistic operating conditions.

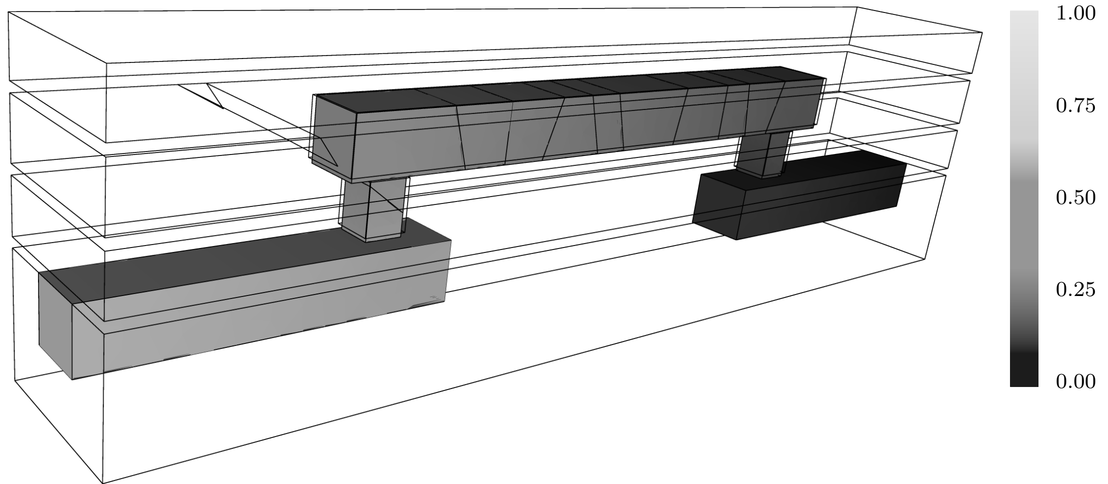

Fig. 6. Electric potential distribution (mV).

VII. Simulation Results and Conclusion

We have applied our model to an interconnect layout which has been extensively used for accelerated electromigration tests [35]. This layout is typical for dual-damascene 0.18 μm technologies. The copper microstructure is set according to results of EBSD (Electron Backscatter Diffraction) measurements [12]. The solution of the electro-thermal problem determines the operating conditions for electromigration simulation. Distributions of the electrical potential and temperature are shown in Fig. 6 and Fig. 7, respectively. All simulations have been performed for the same peak temperature of 673 K at four different current densities: 1 MA/cm^2, 2.5 MA/cm^2, 5 MA/cm^2, and 10 MA/cm^2. The grain boundary, barrier, and capping layer diffusivities are set as $10^4\, D_v$, $10^2\, D_v$, and $10^4\, D_v$, respectively.

The distribution of the peak vacancy concentration for the initial time steps is presented in Fig. 8 and the peak tensile stress in Fig. 9. As one can observe, the peak value of the tensile σ_{yy} stress tensor component, which is orthogonal to the capping layer interface, reaches its maximum at the bottom of the via structure. High values can also be observed at the capping layer interface at two additional positions:

- in the vicinity of a triple point intersection of a grain boundary and the capping layer,
- at the capping layer interface opposite to the via bottom.

Investigations of the given structure reveal that the time behavior of vacancy concentration exhibits two distincive periods.

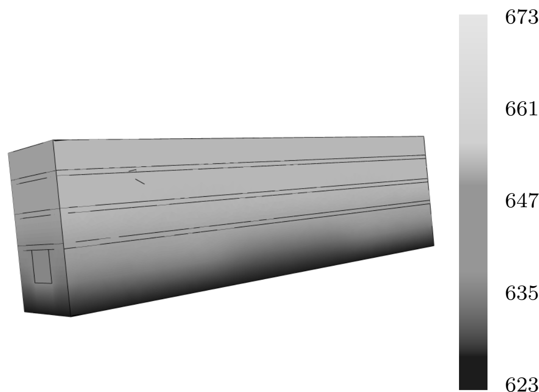

Fig. 7. Temperature distribution (K).

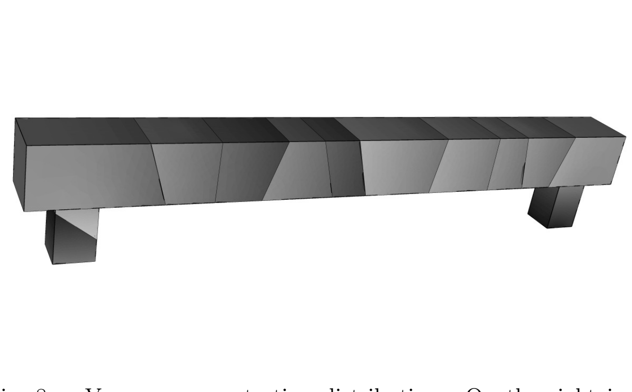

Fig. 8. Vacancy concentration distribution. On the right is the cathode end of the interconnect. Dark areas mark peak values presented in Fig. 11.

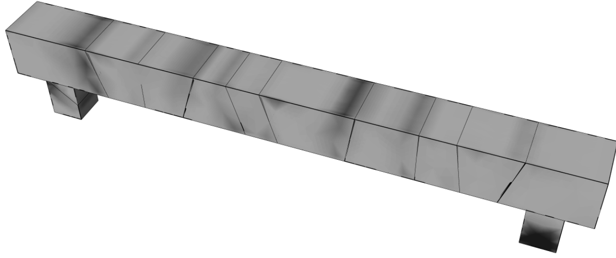

Fig. 9. Peak tensile stress tensor component distribution. Dark areas mark peak values presented in Fig. 12.

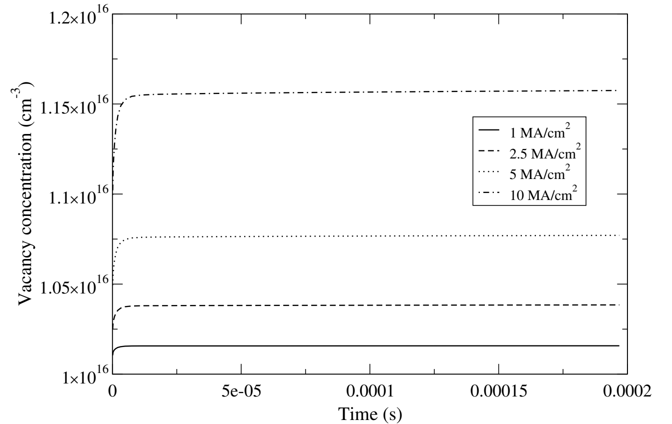

Fig. 10. Early vacancy concentration dynamics.

In the initial shorter period of about 10 ms the vacancy concentration grows from its initial equilibrium value (10^{16} cm^{-3}) value to the peak value (Fig. 10). Later on, in the second period between 1s to 1 hour, the vacancy concentration reduces slightly (Fig. 11). The behavior of stress does not exhibit a similar behavior. The peak stress at the bottom of the via grows continuosly (Fig. 12). This apparent discrepancy can easily be explained by the fact that stress build-up in three-dimensional structures does not correlate with a single local peak vacancy concentration value, but is a result of the net vacancy dynamics in the whole region defined by microstructure and local geometry features. Moreover, we observe that a high tensile stress appears in the neighborhood of triple points (Fig. 10).

For possible void nucleation high tensile stress and a local interface defect are required. Under accelerated test conditions, as used in the presented example, high stresses at the triple points develop in the first hours of testing. As observed in experiments [35] carried out under similar operating conditions, we have the first void nucleation after less than 2 hours.

The maximum of the stress is always at the bottom of the via, but in most cases voids first appear at the capping layer interface [15]. It is obvious that a defect is necessary for void nucleation. The coincidence of high vacancy concentration and high tensile stress regions with triple points indicates that triple points are natural locations of weak adhesion. This assumption was also expressed in the discussion of results of accelerated tests published in [35], [12].

The scenario of weak triple points in combination with a stress threshold would allow multiple void nucleations in a short time, as it has actually already been observed [35].

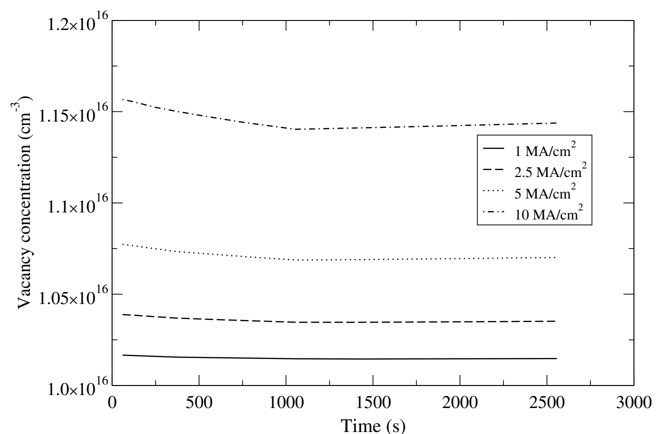

Fig. 11. Late vacancy concentration dynamics.

VIII. Conclusion and Outlook

A comprehensive electromigration model is presented as a basis for a three-dimensional simulation tool. The influence of residual and electromigration induced strains on material transport is discussed and an earlier electromigration model is extended by introduction of tensorial self-diffusivity. The impact of void growth on the resistance of a characteristic interconnect structure is studied and an algorithm for estimation of the void growth time is presented. The physical soundness of the extended electromigration model is verified with several simulation examples. The simulated dynamics of early failure development is in good agreement with experimental observations. The role of triple points for void nucleation is discussed on the basis of simulation and corresponding experimental results. A concept for usage of TCAD tools in combination with experimental tests is presented.

Acknowledgment

Support by the Austrian Science Fund with the project P18825-N14 is gratefully acknowledged.

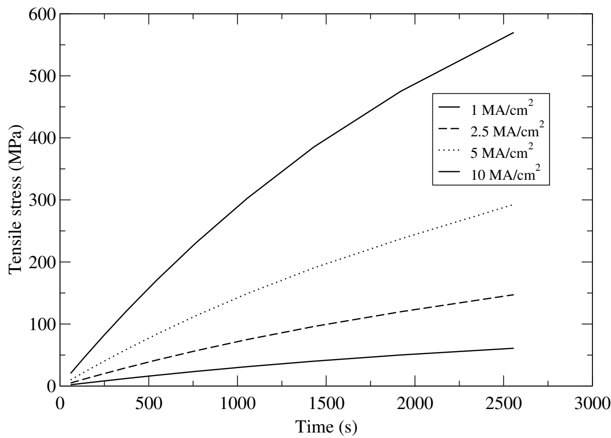

Fig. 12. Peak stress dynamics.

References

[1] I. A. Blech and C. Herring, "Stress Generation by Electromigration," *J. Appl. Phys.*, vol. 29, no. 3, pp. 131–133, 1976.

[2] I. A. Blech, "Electromigration in Thin Aluminum Films on Titanium Nitride," *J. Appl. Phys.*, vol. 47, no. 4, pp. 1203–1208, 1976.

[3] I. A. Blech and K. L. Tai, "Measurement of Stress Gradients Generated by Electromigration," *Appl. Phys. Lett*, vol. 30, no. 8, pp. 387–389, 1976.

[4] W. W. Mullins, "Mass Transport at Interfaces in Single Component Systems," *Metall. Mater. Trans. A (USA)*, vol. 26, no. 8, pp. 1917–1929, 1995.

[5] M. A. Korhonen, P. Borgesen, K. N. Tu, and C. Y. Li, "Stress Evolution due to Electromigration in Confined Metal Lines," *J. Appl. Phys.*, vol. 73, no. 8, pp. 3790–3799, 1993.

[6] J. Lloyd and E. Arzt, "A Simple Model for Stress Voiding in Passivated Thin Film Conductors," *Symposium Proc. on Materials Reliability in Microelectronics II*, vol. 265, pp. 45–57, 1992.

[7] J. Lloyd and J.J.Clement, "Electromigration in Copper Conductors," *Thin Solid Films*, vol. 262, no. 1, pp. 135–141, 1995.

[8] J. J. Clement, "Electromigration Modeling for Integrated Circuit Interconnect Reliability Analysis," *IEEE Trans. on Dev. and Mat. Rel.*, vol. 1, no. 1, pp. 33–42, 2001.

[9] M. E. Sarychev and Y. V. Zhitnikov, "General Model for Mechanical Stress Evolution During Electromigration," *J. Appl. Phys.*, vol. 86, no. 6, pp. 3068 – 3075, 1999.

[10] V. Sukharev, "Simulation of Microstructure Influence on EM-Induced Degradation in Cu Interconnects," *Stress-Induced Phenomena in Metallization: 8th International Workshop, AIP Conference Proceedings*, vol. 944, 2005.

[11] V. Sukharev, R. Choudhury, and C. W. Park, "Physically-Based Simulation of the Early and Long-Term Failures in the Copper Dual Damascene Interconnect," *Integrated Reliability Workshop Final Report, 2003 IEEE International*, pp. 80– 85, 2003.

[12] E. Zschech and V. Sukharev, "Microstructure Effect on EM-Induced Copper Interconnect Degradation," *Microelectronic Engineering*, vol. 82, pp. 629–638, 2005.

[13] R. Rosenberg and M. Ohring, "Void Formation and Growth During Electromigration in Thin Films," *J. Appl. Phys.*, vol. 42, no. 13, pp. 5671–5679, 1971.

[14] M. R. Sorensen, Y. Mishin, and A. F. Voter, "Diffusion Mechanisms in Cu Grain Boundaries," *Phys. Rev. B*, vol. 62, no. 6, pp. 3658–3673, 2000.

[15] J. Lloyd and K. P. Rodbell, "Reliability," *in Handbook of Semiconductor Interconnection Technoogy, edited by G.C. Schwartz and K. V. Srikrishnan*, pp. 471–520, 2006.

[16] P. H. Dederichs and K. Schroeder, "Anisotropic Diffusion in Stress Fields," *Phys. Rev. B*, vol. 17, no. 6, pp. 2524–2536, 1978.

[17] H. Kang, I. Asano, C. Ryu, and S. Wong, "Grain Structure and Electromigration Properties of CVD CU Metallization," *Proceedings of 10th International VLSI Multilevel Interconnection Conference*, pp. 223–229, 1993.

[18] A. von Glasow, "Zuverlässigkeitsaspekte von Kupfermetallisierungen in Integrierten Schaltungen," Dissertation, Technische Universität München, 2005.

[19] E. Zschech, M. A. Meyer, S. G. Mhaisalkar, and A. V. Vairagar, "Effect of Interface Modification on Em-Induced Degradation Mechanisms in Copper Interconnects," *Proceedings of ICMAT 2005 Conference, in press*, 2005.

[20] P. A. Flinn, "Mechanical Stress in VLSI Interconnections: Origins, Effects, Measurement, and Modeling," *MRS Bulletin*, vol. 20, no. 11, pp. 70–73, 1995.

[21] E. Zschech, H.-J. Engelmann, M. Meyer, V. Kahlert, A. V. Vairagar, S. G. Mhaisalkar, A. Krishnamoorthy, M. Yan, K. N. Tu, and V. Sukharev, "Effect of Interface Strength on Electromigrationinduced Inlaid Copper Interconnect degradation: Experiment and Simulation," *Zeitschrift fur Metallkünde*, vol. 96, no. 9, pp. 966–971, 2005.

[22] B. M. Clemens, W. D. Nix, and R. J. Gleixner, "Void Nucleation on a Contaminated Patch," *Journal of Materials Research*, vol. 12, no. 8, pp. 2038–2042, 1997.

[23] R. J. Gleixner, B. M. Clemens, and W. D. Nix, "Void Nucleation in Passivated Interconnect Lines: Effects of Site Geometries, Interfaces, and Interface Flaws," *Journal of Materials Research*, vol. 12, pp. 2081–2090, 1997.

[24] Z. Jing, M. O. Bloomfield, L. Jian-Qiang, R. J. Gutmann, and T. S. Cale, "Modeling Thermal Stresses in 3-D IC Interwafer Interconnects," *IEEE Trans. Sem. Man.*, vol. 19, no. 4, pp. 437–448, 2006.

[25] D. R. Fridline and A. F. Bower, "Influence of Anisotropic Surface Diffusivity on Electromigration Induced Void Migration and Evolution," *J. Appl. Phys.*, vol. 85, no. 6, pp. 3168–3174, 1999.

[26] H. Ceric and S. Selberherr, "An Adaptive Grid Approach for the Simulation of Electromigration Induced Void Migration," *IEICE Trans. Electronics*, no. 3, pp. 421–426, 2002.

[27] D. N. Bhate, A. F. Bower, and A. Kumar, "A Phase Field Model for Failure in Interconnect Lines Due to Coupled Diffusion Mechanisms," *J. Mech. Phys. Solids*, vol. 50, pp. 2057–2083, 2002.

[28] M. Mahadevan and R. Bradley, "Simulations and Theory of Electromigration-Induced Slit Formation in Unpassivated Single-Crystal Metal Lines," *Phys. Rev. B*, vol. 59, no. 16, pp. 11 037–11 046, 1999.

[29] R. Sabelka, "Dreidimensionale Finite Elemente Simulation von Verdrahtungsstrukturen auf Integrierten Schaltungen," Dissertation, Technische Universität Wien, 2001.

[30] C. Harlander, R. Sabelka, R. Minixhofer, and S. Selberherr, "Three-Dimensional Transient Electro-Thermal Simulation," in *Proc. Foreword contributions from thermal investigations of ICs and systems*, 1999, pp. 169–172.

[31] A. S. Oates, "Electromigration Failure of Contacts and Vias in Sub-Micron Integrated Circuit Metallisations," *Microelectron. Reliab.*, vol. 36, no. 7, pp. 925–953, 1996.

[32] S. H. Kang and E. Shin, "A Three-Dimensional Nonlinear Analysis of Electromigration-Induced Resistance Change and Joule Heating in Microelctronics Interconnects," *Solid-State Electronics*, vol. 45, pp. 341–346, 2001.

[33] C. L. Gan, W. Wang, C. V. Thompson, K. L. Pey, W. K. Choi, S. P. Hau-Riege, and B. Yu, "Contrasting Failure Characteristics of Different Levels of Cu Dual-Damascene Metallisation," *Proc. International Symposium on the Physical and Failure Analysis of Integrated Circuits*, pp. 140 – 144, 2002.

[34] M. A. Meyer, M. Herrmann, E. Langer, and E. Zschech, "In Situ SEM Observation of Electromigration Phenomena in Fully Embedded Copper Interconnect Structures," *Microelectronic Engineering*, vol. 64, pp. 375–382, 2002.

[35] A. V. Vairagar, S. G. Mhaisalkar, A. Krishnamoorthy, and K. N. Tu, "In Situ Observation of Electromigration-Induced Void Migration in Dual-Damascene Cu Interconnect Structures," *J. Appl. Phys.*, vol. 85, no. 13, pp. 2502–2504, 2004.